The Histomorphological and Stereological Assessment of Rat Dorsal Root Ganglion Tissues After Various Types of Sciatic Nerve Injury

Burcu Delibaş
Recep Tayyip Erdoğan University
Süleyman KAPLAN (skaplanomu@yahoo.com)
Ondokuz Mayıs University

Research Article

Keywords: Dorsal root ganglion, sciatic nerve injury, stereology, physical disector, unbiased sensory neuron counting

Posted Date: August 1st, 2023

DOI: https://doi.org/10.21203/rs.3.rs-3199786/v1

Additional Declarations: No competing interests reported.

Version of Record: A version of this preprint was published at Histochemistry and Cell Biology on October 19th, 2023. See the published version at https://doi.org/10.1007/s00418-023-02242-0.

Abstract

Peripheral nerve injuries lead to significant changes in the dorsal root ganglia, where the cell bodies of the damaged axons are located. The sensory neurons and the surrounding satellite cells rearrange the composition of the intracellular organelles to enhance their plasticity for adaptation to changing conditions and responding to injury. Meanwhile, satellite cells acquire phagocytic properties and work with macrophages to eliminate degenerated neurons. These structural and functional changes are not identical in all injury types. Understanding the cellular response, which varies according to the type of injury involved, is essential in determining the optimal method of treatment. In this research, we investigated the numerical and morphological changes in primary sensory neurons and satellite cells in the dorsal root ganglion 30 days following chronic compression, crush and transection injuries using stereology, high-resolution light microscopy, immunohistochemistry, and behavioral analysis techniques. Electron microscopic methods were employed to evaluate fine structural alterations in cells. Stereological evaluations revealed no statistically significant difference in terms of mean sensory neuron numbers ($p > 0.05$), although a significant decrease was observed in sensory neuron volumes in the transection and crush injury groups ($p < 0.05$). Active caspase-3 immunopositivity increased in the injury groups compared to the sham group ($p < 0.05$). While crush injury led to desensitization, chronic compression injury caused thermal hyperalgesia. Electromyography parameters exhibited a significant decrease in the compression and crush injury groups compared to the sham group ($p < 0.05$). Macrophage infiltrations were observed in all injury types. Electron microscopic results revealed that the chromatolysis response was triggered in the sensory neuron bodies from the transection injury group. An increase in organelle density was observed in the perikaryon of sensory neurons after crush-type injury. This indicates the presence of a more active regeneration process in crush-type injury than in other types. The effect of chronic compression injury is more devastating than that of crush-type injury, and the edema caused by compression significantly inhibits the regeneration process.

INTRODUCTION

Sensory neurons and satellite cells undergo a series of numerical and morphological alterations following peripheral nerve injury (Muratori et al. 2015; Jager et al. 2020; Lu and Richardson 1993; McKay Hart et al. 2002; Shi et al. 2001; Tandrup and Braendgaard 1994). The location of dorsal root ganglion (DRG) tissues, with their surrounding connective tissue capsule and structure as an isolated pool of neuron bodies, makes them a good model for studying neuronal death or proliferation. Previous studies have shown that the increase in the number of axons occurring after injury in the distal part of the lesion area leads to retrograde alterations in the plasticity of DRG neurons (Mackinnon et al. 1991; Wiberg et al. 2018; Ren et al. 2018). An increase in the surface area of the cell body (Zimmerman et al. 1971) or mitotic proteins released from damaged neurons (Wen et al. 1994) may increase the proliferation of satellite cells. In addition, glial cells in the lesioned area and other cells in the immune system also constitute a component of this response (Jager et al. 2020; Lu and Richardson 1993).

Cellular reorganization after injury in the DRG has attracted the attention of researchers in recent years, and these have focused on cellular and molecular interactions in glial and sensory cells in the DRG following peripheral nerve injury (Chen et al. 2020; Dubovy et al. 2013; Matsumura et al. 2014; Muratori et al. 2015). In addition to such research, there are also stereological and immunohistochemical studies investigating the time-dependent change in cell death and new cell formation in the DRG following peripheral nerve axotomy (McKay Hart et al. 2002; Muratori et al. 2015; Schmalbruch 1987; Shi et al. 2001; Tandrup and Braendgaard 1994). However, the data elicited by different study groups using stereological or non-stereological methods are inconsistent, which has encouraged researchers to conduct more detailed and advanced studies on the subject. In the present study, sensory neuron cell number estimations and volume calculations in the DRG were performed using unbiased stereological methods following the induction of various nerve lesions in Wistar albino rats. The stereological techniques used in the study are reproducible, reliable, and based on purely statistical methods, thus eliminating investigative bias. In addition, this study was intended to elucidate the cellular changes that emerge post-injury by performing detailed electron microscopic analyses at the fine structure level. The cytoplasm and nuclei of somatic sensory neurons and satellite cells in the DRG were evaluated in terms of cytosolic deterioration, distribution of Nissl bodies, and presence of autophagic vacuoles.

The purpose of this study was to investigate cellular changes in the DRG following various types of peripheral nerve injury to primary sensory neurons and satellite cells from a quantitative and ultrastructural perspective. Changes in sensory neuron numbers and satellite cells after injury were investigated using electron microscopic, immunohistochemical, behavioral, electrophysiological, and unbiased stereological methods.

MATERIAL AND METHODS

Experimental groups and surgical procedures

All surgical procedures were performed in the Ondokuz Mayıs University Experimental Animals Research Center, Turkey. Approval (no. 2018/43) was granted by the local ethic committee. Forty-eight male Wistar albino (*Rattus norvegicus domesticus*) rats, 12 weeks old and weighing 200–250 g, were used in the study. General anesthesia was induced by the intraperitoneal administration of 100 mg/kg of ketamine hydrochloride (Ketalar, Parke-Davis, Eczacıbaşı) + 10 mg/kg of xylazine hydrochloride (Rompun). The rat was then fixed on the operating table, and the surgical area was wiped with povidone-iodine scrub (MEDICA brush; 4% chlorhexidine soap, MEDICA BV, the Netherlands) and povidone-iodine (POVIOD; 10% polyvinylpyrrolidone-iodine complex, Saba, Turkey) solution to ensure disinfection.

Following dissection of the biceps femoris muscle of the right leg, the sciatic nerve region 10 mm distal to the extensor digitorum longus muscle was opened. Compression-type injuries were created by means of sutures in one group, and crush-type injuries using 5 1/2-inch hemostatic forceps in another group. Finally, transection injuries were created using a surgical blade in the third group. Following injury

induction, DRG and sciatic nerve tissues at the L4 and L5 levels were removed after waiting for the minimum time (30 days) required for the end of the acute response and Wallerian degeneration.

The animals were divided into four equal groups (n:12):

1. **Sham surgery group (n:12)**: These animals were subjected only to skin incision and general anesthesia. L4 and L5 ganglion tissues were harvested at the end of a 30-day waiting period.
2. **Chronic compression injury group (n:12)**: An experimental chronic compression injury model was established in this group with four loose sutures (5 – 0 chrome catgut) applied to the sciatic nerve at 1-mm intervals. L4 and L5 ganglion tissues were harvested at the end of the 30-day waiting period (Fig. 1a).
3. **Crush injury group (n:12)**: An experimental crush injury model was created in this group using 5 1/2-inch hemostatic forceps (50 N/60 seconds). L4 and L5 ganglion tissues were also harvested at the end of the 30-day waiting period (Fig. 1b).
4. **Transection injury group (n:12)**: An experimental transection injury model was created using a surgical blade. The sciatic nerve was completely transected to prevent reunion between the proximal and distal stumps, and the proximal stump was buried and sutured to the gluteus maximus muscle (Fig. 1c).

Tissue processing steps

Twenty-four (12x2) pieces of L4 and L5 tissues were obtained from the animals of each group. Eighteen (9x2) ganglia were stored in 4% glutaraldehyde + 4% paraformaldehyde solution for embedding in resin, and six (3x2) were stored in 10% formaldehyde solution to yield paraffin blocks. Once the fixation procedures were completed, routine histological processing steps were applied to the tissues placed into formaldehyde. Electron microscopic processing was applied to the tissues placed in glutaraldehyde + paraformaldehyde, after which resin blocks were prepared.

Preparation of samples for electron microscopy and sectioning

Following the electron microscopic tissue processing, 70 nm-thick sections were placed onto copper grids (200 mesh) and contrasted using uranyl acetate–lead citrate solutions for electron microscopic evaluations (JEOL JSM-7001F, JEOL Ltd., Tokyo, Japan). Consecutive 2 µm-thick sections were also placed onto glass slides and stained on a hot plate using a 1% toluidine blue and sodium borate mixture (1 g toluidine blue + 2 g $Na_2B_4O_7{\cdot}10H_2O$ + 100 ml dH_2O) for stereological evaluations.

Stereological evaluations

Estimation of the number of sensory neurons in DRG using the physical disector/ fractionator combination method

Sensory neuron numbers were estimated in consecutive 2 µm-thick sections taken at 50 µm interval using the physical disector/fractionator combination method. The nucleolus of the sensory neurons was selected as a counting criterion. Images from the look-up section were captured at 20x magnification with no area sampling. The analyses were performed using cellSens Entry software with the aid of a light microscope with camera attachment (Olympus, BX43, Center Valley, PA, USA). The regions corresponding to the images captured in the reference section were also identified and photographed at the same magnification. After the cell nucleolus had been selected as the counting criterion, the particle was counted if present in the reference section, but not in the look-up section (Fig. 2). The total number of particles obtained (Q^-) was multiplied by the sampling rates, and the average total number of sensory neurons was calculated using the formula $N = Q^- \times 1/f$.

Evaluation of ganglion tissue volume using the Cavalieri method

The "Cavalieri method," a stereological technique frequently employed for the purpose of volume calculation, was used to evaluate volume changes. This represents a volume calculation method for equally divided parallel structures. The "total sectioned surface area" value obtained by calculating the projected surface areas of the investigated structure on the sampled sections facing the same direction is multiplied by the average section thickness. This yields a volume value for the structure in the examined section images. A pointed grid can be used to measure the area, with each point representing a unit square with a fixed interval (d). The area of the unit square is referred to as the "area associated with the point [**a(p)**]. The section area (A) can be calculated by multiplying the total number of points counted (ΣP) and the area represented by a point [a(p)] (Sonmez et al. 2010) as expressed in the formula:

$$A = \sum P \bullet [a\,(p)]$$

Evaluation of sensory neuron volume

Perikaryon diameter data were used for volume estimations in sensory neurons. Only neurons in which the nucleolus of the cell was seen were taken into account in calculating the diameter of the perikaryon. In order to reduce the type 2 error, four sensory neurons with nucleoli were selected from the counting frame for both small and large-diameter neurons. The area of the tissue in the relevant section was calculated using a point grid. Points separated by areas of 14.63 μm^2 for large-diameter neurons and 5.36 μm^2 for small-diameter neurons were used. Using the diameter (r) value obtained from the mean neuron area data, the average volume was estimated using the 4/3 μr^3 formula. Coefficient of error (CE) and coefficient variation (CV) values for volume and number estimations were calculated according to the formula reported (Gundersen and Jensen 1987)).

Evaluation of immunopositivity for active caspase-3 antibody

The streptavidin-biotin-peroxidase complex (SABPC) technique was used to determine the presence of active caspase-3 (orb500767, Biorbyt, USA) protein in the sections. The primary antibody was diluted (1/200) with phosphate-buffered saline (PBS) at the rate used in previous studies and experiments, as described in the manufacturer's recommendations. An HRP/AEC (ABC) IHC detection kit (ab93705, Abcam) was used for staining, in line with the standard procedure recommended by the manufacturer. Active caspase-3 immunopositivity in the tissue was evaluated semi-quantitatively (Delibas et al. 2022). Briefly, the intensity of the staining was determined on a four-point scale, on which 0 indicated no staining; 1, light staining; 2, moderate staining; and 3, dense staining. One hundred randomly selected neurons were scored in each section. The staining intensities of the cells and the number of cells stained at the same intensity were multiplied and summed in the final step in order to obtain a total immunopositivity score. Immunopositivity scores ranging from 0 to 300 were determined, and statistical evaluations were performed accordingly.

Electrophysiological analysis (Electromyography, EMG)

Electromyographic analyses were applied to measure physiological recovery before the animals were sacrificed. Scope (ver. 3.7.2, AD Instruments, Sydney, Australia) software and a Power Lab 4SP (AD Instruments, Sydney, Australia) device were used for the EMG tests.

The right sciatic nerve was stimulated using bipolar hook electrodes (with a10-mm distance between the anode and cathode parts). The electrodes were placed 10 mm distal to the sciatic notch, after which combined muscle action potentials (amplitude/ latency) were recorded. A grounding electrode was placed on the tail, while the recording electrodes were placed on the middle of the gastrocnemius muscle (approximately 2.5 cm from the simulator). Supramaximal stimuli (10 mV) 0.1 ms in duration were delivered to the sciatic nerve, and the responses were recorded in a quiet room at 22–23°C using an amplifier (PowerLab 4/ 35; ADInstruments, Castle Hill, Australia). The measurements were performed in triplicate for each animal, and action potential curves were evaluated. Finally,mean values were calculated and compared in terms of latency and amplitude.

Hot plate test

The hot plate test was performed on a weekly basis to evaluate cutaneous pain sensitivity. The animals were placed individually onto a surface maintained at 50–56°C, movement being restricted by a Plexiglass cylinder. The time elapsed until the exhibition of hind paw licking and/or waving, and jumping was recorded with a stopwatch. The experiment was terminated after 20 seconds.

Statistical analysis

GraphPad Prism 8.0 software was used for data analysis. Shapiro Wilk normality tests were applied to determine which comparison test to use. The ANOVA test was used to compare more than two homogeneous groups exhibiting normal distribution, while the Welch test was used for non-homogeneous groups. The Kruskal Wallis H test was applied for groups that did not exhibit normal distribution. Tukey’s test was used for normally distributed homogeneous groups, the Tamhane test for

non-homogeneous groups, and the Dunn test for non-normally distributed groups in pairwise comparisons. The repeated measures ANOVA test was applied to compare the measurements performed at different times.

RESULTS

Mean sensory neuron numbers

No significant change was observed in the numbers of sensory neurons in the first 30 days following the various types of sciatic nerve injury ($p > 0.05$) (Table 1; Fig. 3).

Table 1
Mean CE and CV values at stereological analysis of mean sensory neuron numbers, dark and light neuron volumes, and total DRG tissue volumes

		Mean number of sensory neuron (L4)	*Mean number of sensory neuron (L5)*	*Mean number of sensory neuron (L4 + L5)*	*Mean volume of dark sensory neurons*	*Mean volume of light sensory neurons*	*Mean DRG (L4) volume*	*Mean DRG (L5) volume*
Sham	**CE**	0.07	0.09	0.01	0.01	0.02	0.01	0.08
	CV	0.18	0.19	0.2	0.15	0.17	0.25	0.21
CCI	**CE**	0.07	0.08	0.03	0.01	0.02	0.01	0.01
	CV	0.16	0.22	0.19	0.17	0.07	0.23	0.10
Crush	**CE**	0.07	0.07	0.05	0.01	0.02	0.01	0.01
	CV	0.23	0.18	0.18	0.20	0.10	0.20	0.24
Transection	**CE**	0.09	0.07	0.05	0.01	0.03	0.01	0.01
	CV	0.24	0.25	0.28	0.23	0.16	0.13	0.26

Mean dark and light sensory neuron volumes

A significant decrease was observed in the sensory neuron perikaryon volume of the dark sensory neurons in the transection group compared with the sham group ($p < 0,01$). However, no significant difference was found between the chronic compression injury and sham groups, or between the crush and sham groups ($p \geq 0.05$) (Fig. 4).

A statistically significant difference was observed between the crush and sham ($p < 0.05$) and transection and sham groups ($p < 0.01$). No difference was determined between the chronic compression injury and sham groups ($p \geq 0.05$) (Fig. 4).

Total mean ganglion tissue volumes

Although no significant difference was observed in L4 level DRG volumes in the injury groups compared with the sham group, a decreasing tendency was determined in the transection group. No difference was found between any of the groups in terms of L5 ganglion tissue volumes ($p \geq 0.05$) (Fig. 4).

Electrophysiological analysis (EMG) results

Data and graphs for electrophysiological measurements are shown below (Tables 2–3; Fig. 5).

Table 2
Compound action potential amplitude findings. Data are presented as mean and standard error of the mean (SEM)

	Mean ± SEM (mV)	CV (%)	Test statistics	p
Sham[a]	51,91 ± 6,08	11,72	10,646	0,000*
CCI[b]	34,45 ± 10,31	29,95		
Crush injury[b]	41,58 ± 10,46	25,17		

Table 3
Compound action potential latency findings. Data are presented as mean and standard error of the mean (SEM)

	Mean ± SEM (s)	CV (%)	Median	Min.-Max.	Test statistics	p
Sham[a]	0,47 ± 0,15	31,94	0,45	0,28 – 0,71	23,381	0,000*
CCI[b]	2,05 ± 0,40	19,58	2,01	1,27 – 2,97		
Crush injury[b]	1,93 ± 0,44	23,01	2,17	1,22 – 2,36		

Latency values differed significantly between the sham group and the other groups ($p < 0.001$). Significant differences were also observed between the sham group and the chronic compression injury group ($p < 0.001$) and between the sham group and the crush injury group ($p < 0.024$).

Hot Plate Test Results

The data and a graph for the hot plate test are given below (Table 4, Fig. 6).

Table 4
Hot plate test findings. Data are presented as mean and SEM (SEM: standard error of the mean)

Week	Group	Mean	SEM	Test statistics (Week) (Injury)	p
Week 1	Sham[a]	8,07	0,71	2,334	0,079
	CCI[b]	5,90	0,54	227,93	0,000*
	Crush injury[b]	12,82	0,97		
Week 2	Sham[a]	8,81	0,64		
	CCI[b]	4,81	0,40		
	Crush injury[b]	13,18	0,94		
Week 3	Sham[a]	8,72	0,44		
	CCI[b]	3,81	0,29		
	Crush injury[b]	12,27	0,68		
Week 4	Sham[a]	9	0,53		
	CCI[b]	4,63	0,92		
	Crush injury[b]	9,27	0,48		

No difference was determined between the groups when these were evaluated on a weekly basis ($p > 0.05$). When the weeks were evaluated within themselves, a significant difference emerged between the sham group and the other groups on a weekly basis ($p < 0.05$). No difference was observed between the crush and compression injury groups ($p > 0.05$).

Immunohistochemical results

Immunohistochemical staining of DRG tissue with the active form of caspase-3, one of the apoptosis precursor proteins, revealed cytoplasmic immunopositivity in some neurons (Fig. 7). The results showed a significant increase in active caspase-3 immunopositivity in all the injury groups in comparison to the sham group ($p < 0.05$) whereas the differences between the various injury types were not significant ($p > 0.05$). The results are given below (Table 5, Fig. 8).

Table 5
Immunohistochemical scores for active caspase-3 staining (mean ± standard error of mean (SEM)) Coefficient of variation (CV)

	Mean ± SEM (mV)	CV (%)	Test statistics	p
Sham[a]	103,00 ± 26,51	25,74	8,301	0,008*
CCI[b]	180,33 ± 6,50	3,60		
Crush injury [b]	163,66 ± 15,17	9,27		
Transection injury [b]	170,66 ± 28,11	16,47		

Ultrastructural alterations following the various injury types

Light microscopic results

Light microscopic evaluations revealed intact sensory neurons and satellite cells surrounding them in the sham group. The sensory neuron nuclei were centrally located, and the nuclear membrane was well preserved. Satellite cells surrounded the sensory neurons in the form of a thin membrane and exhibited a normal morphology. Few phagocytic cells were observed in the intercellular area (Fig. 9a, b, c). Light microscopic images from the chronic compression injury group revealed a normal morphological structure in the sensory neurons and the satellite cells surrounding them. Hypertrophy was detected in satellite cells surrounding some sensory neurons. Disruption of cell integrity and indentation in the nucleus were evident in some neurons. Regional deteriorations were seen in the axons (Fig. 9d, e, f). The crush injury group images revealed a noteworthy increase in the number of phagocytic cells. Additionally, marked morphological deteriorations were present in sensory neurons and satellite cells. In addition to regional disruptions in the cell and nuclear membranes of sensory neurons, large areas of vacuolization were detected in their cytoplasm. Diffuse hypertrophy was seen in satellite cells. In addition, cytoplasmic extensions were also evident, extending from the satellite cells towards the sensory neurons, and the satellite cells exhibited a phagocytic cell-like structure. Regional deteriorations were evident in the myelin sheath structure of the axons (Fig. 9g, h, ı). Light microscopic photographs from the transection group revealed morphological damage in some neurons and satellite cells. Additionally, an increased number of phagocytic cells was observed. One particularly noteworthy finding was that satellite cells surrounding some sensory neurons produced cytoplasmic extensions towards the sensory neuron cytoplasm. The nuclear membrane integrity of sensory neurons was disrupted, and marked indentation was evident in the nucleus. Numerous phagocytic cells appeared in the intercellular environment. In addition to the wide areas of vacuolization seen in sensory neurons, such areas were also present in some satellite cells (Fig. 9j, k, l).

Electron microscopic results

Electron microscopic ultrastructural analyses of tissues from the sham group revealed a normal morphology in the sensory neurons and the satellite cells. Tightly intertwined regions of interdigitation were observed between satellite cells and sensory neurons. Few phagocytic cells were observed in the intercellular area. The nuclei of sensory neurons were generally located centrally, and the structural integrity of the nuclear membrane was preserved. Nissl bodies were homogeneously distributed in the cytoplasm of sensory neurons. Examination of mitochondria in the cytoplasm of sensory neurons and satellite cells revealed that the inner and outer membrane and cristae structures were all well preserved (Fig. 10).

Electron microscopic ultrastructural analyses of the tissues from the chronic compression injury group revealed an increase in the numbers of phagocytic cells in the intercellular area. The nuclear membrane was well preserved. Round-shaped electron-dense bodies were noted in the cytoplasm of some sensory neurons. Lipid droplets were also observed in the cytoplasm of electron-dense bodies (Fig. 11).

Electron microscopic ultrastructural analyses of specimens from the crush injury group showed deterioration in the membrane structures of the sensory neuron nuclei and the satellite cells surrounding them. Autophagic vacuoles and electron-dense bodies were seen in the cytoplasm of sensory neurons. High-magnification examination of the electron-dense bodies revealed lamellar structures and lipid droplets. Structural deformations were seen in the organelles of the sensory neurons and satellite cells. An increased mitochondrial volume, deterioration in mitochondrial membrane structure and crystals, and changes in the distribution of Nissl bodies were observed. Other pathological changes included structural impairement in the cytoplasm of sensory neurons and disruption of the structural integrity of sensory neuron cell membranes (Fig. 12).

Electron microscopic ultrastructural analyses of tissues from the transection group revealed significant alterations and reorganizations in the organelles compared to the other groups. A noticeable increase in phagocytic cell numbers was detected in the intracellular environment. In addition, increases in volume and also in organelle density were observed in satellite cells surrounding sensory neurons. The nucleus was in an eccentric position in some of the neurons. Examination of the cytoplasm of the satellite cells surrounding the sensory neurons revealed numerous filled autophagic vacuoles. Rearrangements in the structures responsible for protein synthesis were observed, and Nissl bodies were translocated eccentrically toward the periphery of the cell (chromatolysis). Satellite cells exhibited multilayered folding patterns. Evaluation of the axons revealed ballooning in the myelin sheath and deteriorations in the myelin sheath structure. Electron-dense bodies were seen in the cytoplasm of some sensory neurons. The integrity of the nucleus was disrupted in some sensory neurons, and vacuolization in the cytoplasm was widely dispersed in large areas (Figs. 13, 14, 15).

DISCUSSION

This study investigated the effect of various types of sciatic nerve injury on the DRG using qualitative and quantitative methods. In addition to stereological analyses of sensory neurons, the nuclei and cytoplasm

of neurons and satellite cells were examined at the ultrastructural level using electron microscopy.

Poor clinical recovery after injury is attributed to sensory neuron death occurring after peripheral nerve lesions (McKay Hart et al. 2002; Groves et al. 2003; Liss et al. 1994). A previous study reported sensory neuron loss rates of 24% on the seventh day and 54% on the 28th day after sciatic nerve transection injury without reunion of the freed ends (Shi et al. 2001). Similarly, Groves et al. reported significant sensory neuron loss 30 days after sciatic nerve injury in Sprague-Dawley rats (Groves et al. 2003). Tandrup et al. reported that numbers of sensory neurons tended to decrease in the fourth week after injury, although the difference was not statistically significant (Tandrup et al. 2000). Similar to that study, although we observed a decrease in the number of neurons in the fourth week after transection injury in the present study, that finding was not statistically significant. Similarly, Lekan et al. reported that the decrease in the numbers of neurons as a result of the fifth and sixth lumbar segmental nerve lesions commenced from the sixth week (Lekan et al. 1997). At electron microscopic analysis, although we obtained images indicating apoptosis, necrosis, and autophagocytosis, the process was still in the initial stages.

There are also spinal nerve injury studies which have reported neuronal losses (Feringa et al. 1985; Vestergaard et al. 1997). Jakobsen et al. showed that the decrease in the number of sensory neurons became statistically significant after the 15th day following spinal nerve axotomy performed 7 mm distal to the L5 level DRG (Vestergaard et al. 1997). In another study conducted by the same study group, a statistically significant decrease was reported from the fourth day after crush injury to the same region (Degn et al. 1999). It may therefore be concluded that more dramatic losses can be observed when the lesion area is located close to the ganglion. Some studies conducted with compression injury and crush injuries have reported statistically significant neuronal losses (Noorafshan et al. 2011). However, Muratori et al. observed a 42% increase in the number of sensory neurons on the 30th day following peripheral nerve crush injury to the terminal branches of the brachial plexus (Muratori et al. 2015). In accordance with that study reporting post-traumatic neurogenesis, we also observed an increase in the numbers of neurons after crush and compression injuries in the present study, although the results were not statistically significant. The reason for this may be that the brachial plexus is located closer to the cell bodies compared to the sciatic nerve, and that cellular proliferation can therefore be observed without delay as a result of faster anterograde and retrograde transports. Consistent with these results, the crush and compression injury groups were rich in rough endoplasmic reticulum, mitochondria, and Golgi body organelles on electron microscopic images. These results indicate that cellular proliferation was triggered more in the crush and compression injury groups than in the transection injury group. The continuity of the axonal bridge between the distal and proximal parts of the nerve in crush and compression injuries ensures the continuity of the signals carried retrogradely from the lesioned area. In support of this phenomenon, a study by Hart et al. showed a decrease in the number of TUNEL-positive neurons when nerve regeneration occurs. Likewise, a 21% neuronal loss was reported in the absence of axonal repair after the injury, decreasing to 12% when repair is performed with a delay of one week after the injury, and minimal neuron loss (4%) when the repair is performed immediately after the injury (McKay Hart et al.

2002). All these studies reveal that neurotrophic factors released from the distal stump after injury are the main factor determining cell death rates.

Very few studies have investigated the total DRG volume after injury, and analyses have mostly been performed using the Cavalieri method (Gundersen and Jensen 1987). Hart et al. reported a 19% volume loss compared to a control group after peripheral axotomy (McKay Hart et al. 2002). In the present study, although a tendency to volume decrease was observed in the transection group, the difference was not statistically significant. Atrophy of the total tissue volume at the L4 level after transection injury may reflect the insufficiency of growth factors, as well as a decrease in mean perikaryon volume as a result of severe injury.

Ultrastructural evaluation of cellular changes following various types of injury

The neuron-glia complex surrounded by the perineural sheath can be regarded as a separate functional and structural unit (Pannese 1981). The satellite cell, which is associated with the sensory neuron cell, has been shown to respond synchronously to various pathological conditions. Electron microscopic studies have revealed that the volume increase in sensory neurons is also reflected in satellite cells (Pannese et al. 1972; Pannese et al. 1975). The present study showed a weakening of the physical connection between the sensory neuron and the satellite cell, especially after transection injury. The connection between the two was weakened or even severed in places, especially in the transection injury group. The weakening of this connection interrupts the metabolic support between satellite cells and neurons, disrupting the ion passage balance and the traffic of substances entering and leaving the neuron, and resulting in loss of the protective function of the satellite cell on the sensory neuron (Pannese 1981; Martinelli et al. 2005; Thippeswamy et al. 2005).

Researchers have stated that glial cells that acquire phagocytic characteristics exhibit hypertrophic features and are characterized by containing lysosome-like bodies and increased numbers of mitochondria, as well as lamellar bodies and residues as a result of neuronal degeneration (Cantera and Technau 1996). Consistent with these data, we also observed a significant increase in satellite cell volume in the injured groups in this study (although no quantitative measurement parameter was used). In addition, an increase in the numbers of mitochondria and other organelles was observed in the cytoplasm of satellite cells. The increase in neuronal debris and accumulation of lipofuscin materials in the cytoplasm also indicate that these cells perform phagocytosis.

Satellite cells surround the sensory neurons to form multiple layers following transection injury

Numerous areas of invagination were visible at the connection surface between neurons and satellite cells. These invaginations appear as membrane-limited structures with low electron density. A large number of invaginations were found in the connection surface rich in gap junctions between satellite

cells and neurons in the transection injury group in this study. Meanwhile, the satellite cells in the transection injury group surrounded the sensory neurons in such a way to form multiple layers. The same layering pattern was not observed in the crush or chronic compression injury groups. Similar results were obtained in a previous study that examined the rat DRG following various types of sciatic nerve injury (Arkhipova et al. 2010). The results demonstrated that in normal conditions, satellite cells surround the neuron in the form of a single, thin layer. Interestingly, the number of layers increased to more than two in the transection injury group, and the extensions of the satellite cells extended and branched to neighboring neurons. This finding, observed in both previous research and the present study reveals post-traumatic regeneration by increasing the connection surface area between the neuron and satellite cell.

Transection injury triggers a chromatolysis response in sensory neuron bodies

A chromatolysis response occurs following peripheral nerve injuries. This can be easily distinguished under light microscopy. This event essentially leads to changes in the location, aggregation, and organization of Nissl bodies (Lieberman 1971). Electron microscopic studies have shown marked dispersion of polyribosomal structures and fragmentation of rough endoplasmic reticulum structures as a result of chromatolysis (Barron et al. 1976; Cragg 1970; Dentinger et al. 1979). Another important cellular response that occurs in the chromatolysis response is the migration of the remaining ribonucleoprotein complexes toward the periphery of the cell body and the eccentric translocation of the nucleus in the cytoplasm (Cragg 1970; Barron et al. 1976; Dentinger et al. 1979; Johnson and Sears 2013). In summary, chromatolysis can be defined as the reorganization of the main components involved in protein synthesis in the cytoplasm (Lieberman 1971). The post-lesion chromatolytic event in the sensory neurons is not seen in all types of injury (Claman and Bernstein 1981). The occurrence of chromatolysis may vary depending on the age of the subjects, as well as the severity of the damage (e.g., crushing, compression or transection) and the distance of the damaged area from the cell body (Barron 2004; Goldstein et al. 1987). At the same time, protein synthesis increases in cases in which the anabolic response is fast and strong, and even if chromatolysis is observed, catabolic processes do not cause protein degradation. The intense active caspase-3 immunopositivity observed in injured groups can therefore be attributed to the increased activity of various nucleases and proteases. Various activated caspases degrade nuclear substrates such as lamin and cytoplasmic proteins such as fodrin and actin (Chang and Yang 2000; Martelli et al. 1997). All these protein degradations lead to the fragmentation of the cellular structures. The fact that we encountered chromatolyzed neurons only in the transection injury group in this study also appears to confirm this. The investigation of ribonucleases that cause degradation of free polyribosomes or monoribosomes is important for the development of therapeutic strategies in axotomized neurons.

In conclusion, the results indicate that response to transection type injury differs with same aspects from other injury types. The interruption between the distal and proximal stump of the nerve leads to increased plasticity in sensory neurons and glial cells and macrophage-like behaviors (such as autophagosome formation) in the satellite cells. These changes reveal the flexibility of glial cells in the tissue.

Declarations

ACKNOWLEDGEMENTS

The authors report no conflicts of interest.

Funding

This study was funded by the Project Management Office of Ondokuz Mayıs University (Suleyman Kaplan) (PYO.TIP.1904.20.006).

Author information

Department of Histology and Embryology, Faculty of Medicine, Recep Tayyip Erdogan University, Rize, Turkey, Burcu Delibaş

Department of Histology and Embryology, Faculty of Medicine, Ondokuz Mayıs University, Samsun, Turkey, Süleyman Kaplan

Contributions

B.D. conceived and designed the study, performed the experiment, and analyzed the data under the supervision of S.K. The funding acquisition and administered all stages of the project were managed by S.K. The authors of this work contributed towards the interpretation of findings from this study, done a role in drafting the article and revising it critically for its intellectual content, and gave their final approval for this version of the paper to be published.

References

1. Arkhipova SS, Raginov IS, Mukhitov AR, Chelyshev YA (2010) Satellite cells of sensory neurons after various types of sciatic nerve trauma in the rat. Neurosci Behav Physiol 40 (6):609-614. doi:10.1007/s11055-010-9303-7
2. Barron KD (2004) The axotomy response. J Neurol Sci 220 (1-2):119-121. doi:10.1016/j.jns.2004.03.009
3. Barron KD, Dentinger MP, Nelson LR, Scheibly ME (1976) Incorporation of tritiated leucine by axotomized rubral neurons. Brain Res 116 (2):251-266. doi:10.1016/0006-8993(76)90903-3
4. Cantera R, Technau GM (1996) Glial cells phagocytose neuronal debris during the metamorphosis of the central nervous system in Drosophila melanogaster. Dev Genes Evol 206 (4):277-280. doi:10.1007/s004270050052
5. Chang HY, Yang X (2000) Proteases for cell suicide: functions and regulation of caspases. Microbiol Mol Biol Rev 64 (4):821-846. doi:10.1128/MMBR.64.4.821-846.2000

6. Chen B, Carr L, Dun XP (2020) Dynamic expression of Slit1-3 and Robo1-2 in the mouse peripheral nervous system after injury. Neural Regen Res 15 (5):948-958. doi:10.4103/1673-5374.268930
7. Claman DL, Bernstein JJ (1981) Heterogeneous Reaction of Cortical Layer Vb Neurons to Pyramidotomy. Anat Rec 199 (3):A53-A53
8. Cragg BG (1970) What is the signal for chromatolysis? Brain Res 23 (1):1-21. doi:10.1016/0006-8993(70)90345-8
9. Degn J, Tandrup T, Jakobsen J (1999) Effect of nerve crush on perikaryal number and volume of neurons in adult rat dorsal root ganglion. J Comp Neurol 412 (1):186-192. doi:10.1002/(sici)1096-9861(19990913)412:1<186::aid-cne14>3.0.co;2-h
10. Delibas B, Kaplan AA, Marangoz AH, Eltahir MI, Altun G, Kaplan S (2022) The effect of dietary sesame oil and ginger oil as antioxidants in the adult rat dorsal root ganglia after peripheral nerve crush injury. Int J Neurosci:1-11. doi:10.1080/00207454.2022.2145475
11. Dentinger MP, Barron KD, Kohberger RC, McLean B (1979) Cytologic observations on axotomized feline Betz cells. II. Quantitative ultrastructural findings. J Neuropathol Exp Neurol 38 (5):551-564. doi:10.1097/00005072-197909000-00008
12. Dubovy P, Brazda V, Klusakova I, Hradilova-Svizenska I (2013) Bilateral elevation of interleukin-6 protein and mRNA in both lumbar and cervical dorsal root ganglia following unilateral chronic compression injury of the sciatic nerve. J Neuroinflamm 10. doi:Artn 55 10.1186/1742-2094-10-55
13. Feringa ER, Lee GW, Vahlsing HL, Gilbertie WJ (1985) Cell death in the adult rat dorsal root ganglion after hind limb amputation, spinal cord transection, or both operations. Exp Neurol 87 (2):349-357. doi:10.1016/0014-4886(85)90225-0
14. Goldstein ME, Cooper HS, Bruce J, Carden MJ, Lee VM, Schlaepfer WW (1987) Phosphorylation of neurofilament proteins and chromatolysis following transection of rat sciatic nerve. J Neurosci 7 (5):1586-1594. doi:10.1523/JNEUROSCI.07-05-01586.1987
15. Groves MJ, Schanzer A, Simpson AJ, An SF, Kuo LT, Scaravilli F (2003) Profile of adult rat sensory neuron loss, apoptosis and replacement after sciatic nerve crush. J Neurocytol 32 (2):113-122. doi:10.1023/b:neur.0000005596.88385.ec
16. Gundersen HJ, Jensen EB (1987) The efficiency of systematic sampling in stereology and its prediction. J Microsc 147 (Pt 3):229-263. doi:10.1111/j.1365-2818.1987.tb02837.x
17. Jager SE, Pallesen LT, Richner M, Harley P, Hore Z, McMahon S, Denk F, Vaegter CB (2020) Changes in the transcriptional fingerprint of satellite glial cells following peripheral nerve injury. Glia 68 (7):1375-1395. doi:10.1002/glia.23785
18. Johnson IP, Sears TA (2013) Target-dependence of sensory neurons: an ultrastructural comparison of axotomised dorsal root ganglion neurons with allowed or denied reinnervation of peripheral targets. Neuroscience 228:163-178. doi:10.1016/j.neuroscience.2012.10.015
19. Lekan HA, Chung K, Yoon YW, Chung JM, Coggeshall RE (1997) Loss of dorsal root ganglion cells concomitant with dorsal root axon sprouting following segmental nerve lesions. Neuroscience 81 (2):527-534. doi:10.1016/s0306-4522(97)00173-5

20. Lieberman AR (1971) The axon reaction: a review of the principal features of perikaryal responses to axon injury. Int Rev Neurobiol 14:49-124. doi:10.1016/s0074-7742(08)60183-x
21. Liss AG, af Ekenstam FW, Wiberg M (1994) Cell loss in sensory ganglia after peripheral nerve injury. An anatomical tracer study using lectin-coupled horseradish peroxidase in cats. Scand J Plast Reconstr Surg Hand Surg 28 (3):177-188. doi:10.3109/02844319409015978
22. Lu X, Richardson PM (1993) Responses of macrophages in rat dorsal root ganglia following peripheral nerve injury. J Neurocytol 22 (5):334-341. doi:10.1007/BF01195557
23. Mackinnon SE, Dellon AL, Obrien JP (1991) Changes in Nerve-Fiber Numbers Distal to a Nerve Repair in the Rat Sciatic-Nerve Model. Muscle & Nerve 14 (11):1116-1122. doi:DOI 10.1002/mus.880141113
24. Martelli AM, Bareggi R, Bortul R, Grill V, Narducci P, Zweyer M (1997) The nuclear matrix and apoptosis. Histochem Cell Biol 108 (1):1-10. doi:10.1007/s004180050140
25. Martinelli C, Sartori P, De Palo S, Ledda M, Pannese E (2005) Increase in number of the gap junctions between satellite neuroglial cells during lifetime: An ultrastructural study in rabbit spinal ganglia from youth to extremely advanced age. Brain Res Bull 67 (1-2):19-23. doi:10.1016/j.brainresbull.2005.05.021
26. Matsumura Y, Yokoyama Y, Hirakawa H, Shigeto T, Futagami M, Mizunuma H (2014) The prophylactic effects of a traditional Japanese medicine, goshajinkigan, on paclitaxel-induced peripheral neuropathy and its mechanism of action. Mol Pain 10:61. doi:10.1186/1744-8069-10-61
27. McKay Hart A, Brannstrom T, Wiberg M, Terenghi G (2002) Primary sensory neurons and satellite cells after peripheral axotomy in the adult rat: timecourse of cell death and elimination. Exp Brain Res 142 (3):308-318. doi:10.1007/s00221-001-0929-0
28. Muratori L, Ronchi G, Raimondo S, Geuna S, Giacobini-Robecchi MG, Fornaro M (2015) Generation of new neurons in dorsal root Ganglia in adult rats after peripheral nerve crush injury. Neural Plast 2015:860546. doi:10.1155/2015/860546
29. Noorafshan A, Omidi A, Karbalay-Doust S (2011) Curcumin protects the dorsal root ganglion and sciatic nerve after crush in rat. Pathol Res Pract 207 (9):577-582. doi:10.1016/j.prp.2011.06.011
30. Pannese E (1981) The satellite cells of the sensory ganglia. Adv Anat Embryol Cell Biol 65:1-111. doi:10.1007/978-3-642-67750-2
31. Pannese E, Bianchi R, Calligaris B, Ventura R, Weibel ER (1972) Quantitative relationships between nerve and satellite cells in spinal ganglia. An electron microscopical study. I. Mammals. Brain Res 46:215-234. doi:10.1016/0006-8993(72)90017-0
32. Pannese E, Ventura R, Bianchi R (1975) Quantitative relationships between nerve and satellite cells in spinal ganglia: an electron microscopical study. II. Reptiles. J Comp Neurol 160 (4):463-476. doi:10.1002/cne.901600404
33. Ren H, Jin HL, Jia ZP, Ji N, Luo F (2018) Pulsed Radiofrequency Applied to the Sciatic Nerve Improves Neuropathic Pain by Down-regulating The Expression of Calcitonin Gene-related Peptide in the Dorsal Root Ganglion. International Journal of Medical Sciences 15 (2):153-160. doi:10.7150/ijms.20501

34. Schmalbruch H (1987) The number of neurons in dorsal root ganglia L4-L6 of the rat. Anat Rec 219 (3):315-322. doi:10.1002/ar.1092190313
35. Shi TJ, Tandrup T, Bergman E, Xu ZQ, Ulfhake B, Hokfelt T (2001) Effect of peripheral nerve injury on dorsal root ganglion neurons in the C57 BL/6J mouse: marked changes both in cell numbers and neuropeptide expression. Neuroscience 105 (1):249-263. doi:10.1016/s0306-4522(01)00148-8
36. Sonmez OF, Odaci E, Bas O, Colakoglu S, Sahin B, Bilgic S, Kaplan S (2010) A stereological study of MRI and the Cavalieri principle combined for diagnosis and monitoring of brain tumor volume. Journal of Clinical Neuroscience 17 (12):1499-1502. doi:10.1016/j.jocn.2010.03.044
37. Tandrup T, Braendgaard H (1994) Number and volume of rat dorsal root ganglion cells in acrylamide intoxication. J Neurocytol 23 (4):242-248. doi:10.1007/BF01275528
38. Tandrup T, Woolf CJ, Coggeshall RE (2000) Delayed loss of small dorsal root ganglion cells after transection of the rat sciatic nerve. J Comp Neurol 422 (2):172-180. doi:10.1002/(sici)1096-9861(20000626)422:2<172::aid-cne2>3.0.co;2-h
39. Thippeswamy T, McKay JS, Morris R, Quinn J, Wong LF, Murphy D (2005) Glial-mediated neuroprotection: evidence for the protective role of the NO-cGMP pathway via neuron-glial communication in the peripheral nervous system. Glia 49 (2):197-210. doi:10.1002/glia.20105
40. Vestergaard S, Tandrup T, Jakobsen J (1997) Effect of permanent axotomy on number and volume of dorsal root ganglion cell bodies. J Comp Neurol 388 (2):307-312
41. Wen JY, Morshead CM, van der Kooy D (1994) Satellite cell proliferation in the adult rat trigeminal ganglion results from the release of a mitogenic protein from explanted sensory neurons. J Cell Biol 124 (6):1005-1015. doi:10.1083/jcb.124.6.1005
42. Wiberg R, Novikova LN, Kingham PJ (2018) Evaluation of apoptotic pathways in dorsal root ganglion neurons following peripheral nerve injury. Neuroreport 29 (9):779-785. doi:10.1097/Wnr.0000000000001031
43. Zimmerman E, Karsh D, Humbertson A, Jr. (1971) Initiating factors in perineuronal cell hyperplasia associated with chromatolytic neurons. Z Zellforsch Mikrosk Anat 114 (1):73-82. doi:10.1007/BF00339466

Figures

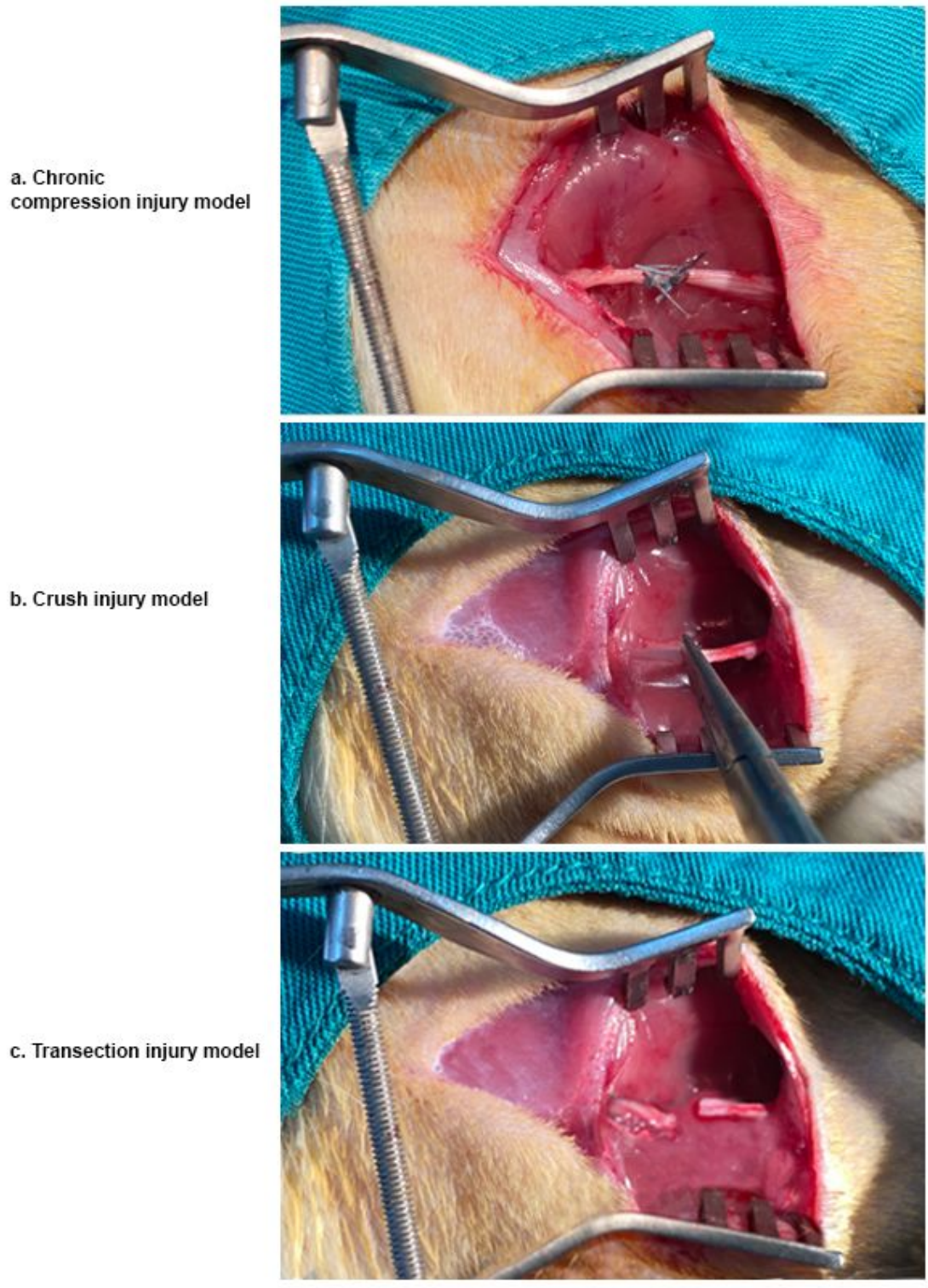

Figure 1

Sciatic nerve injury models. (a) Chronic compression injury. (b) Crush injury. (c) Transection injury

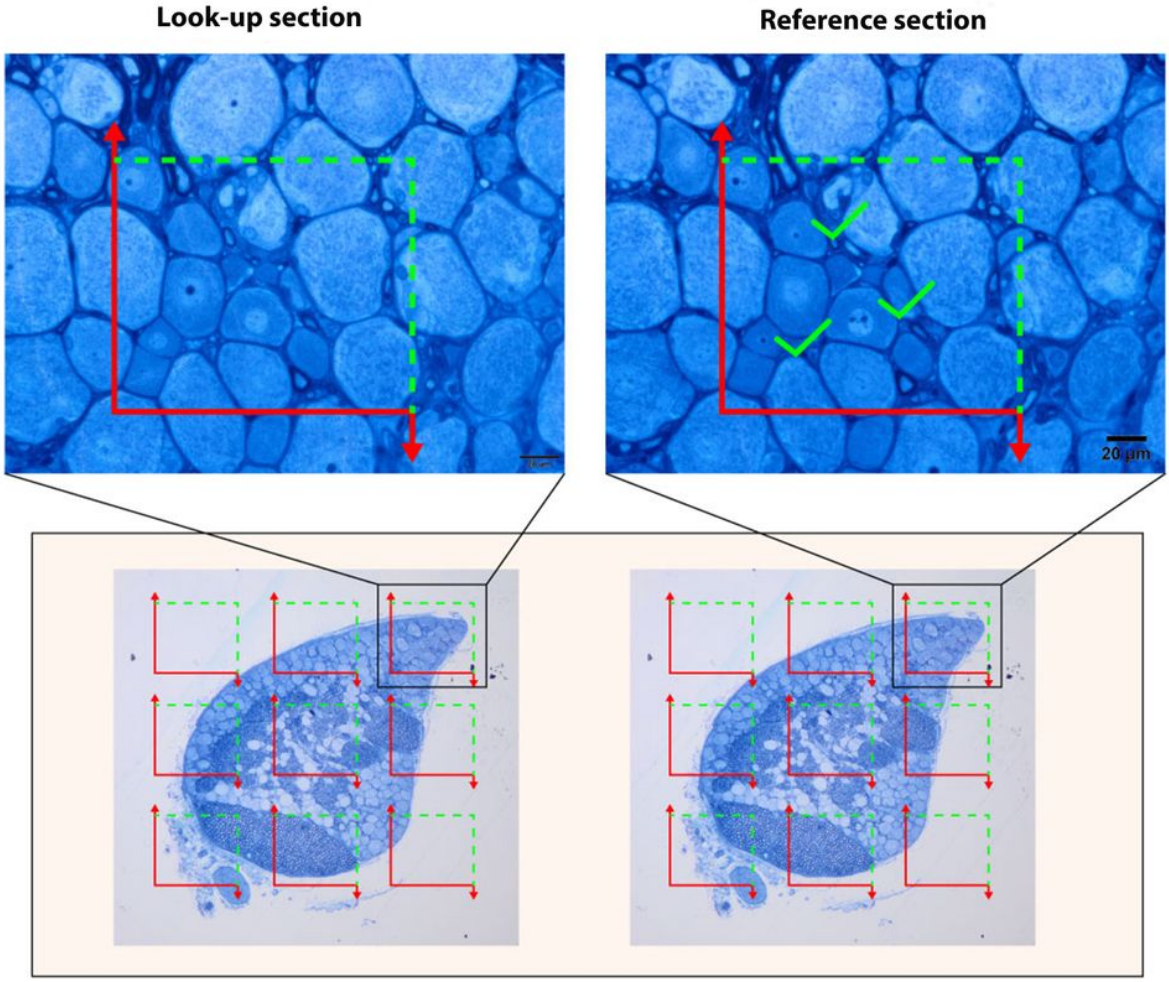

Figure 2

Application of the physical disector technique to consecutive sections. Countable particles are indicated by (√) inside the counting frame (toluidine blue staining)

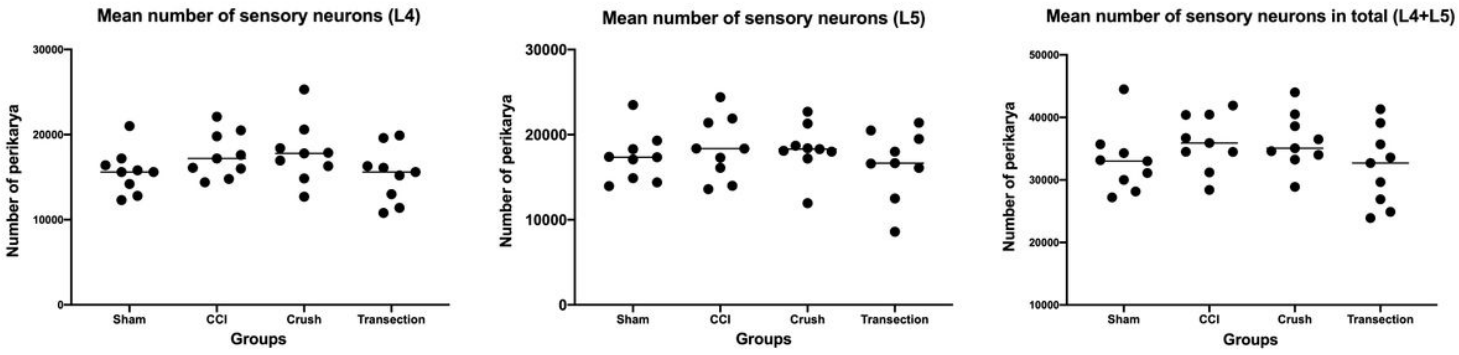

Figure 3

Mean numbers of sensory neurons in L4 and L5 level DRG tissues, and the total number of neurons at the L4+L5 level

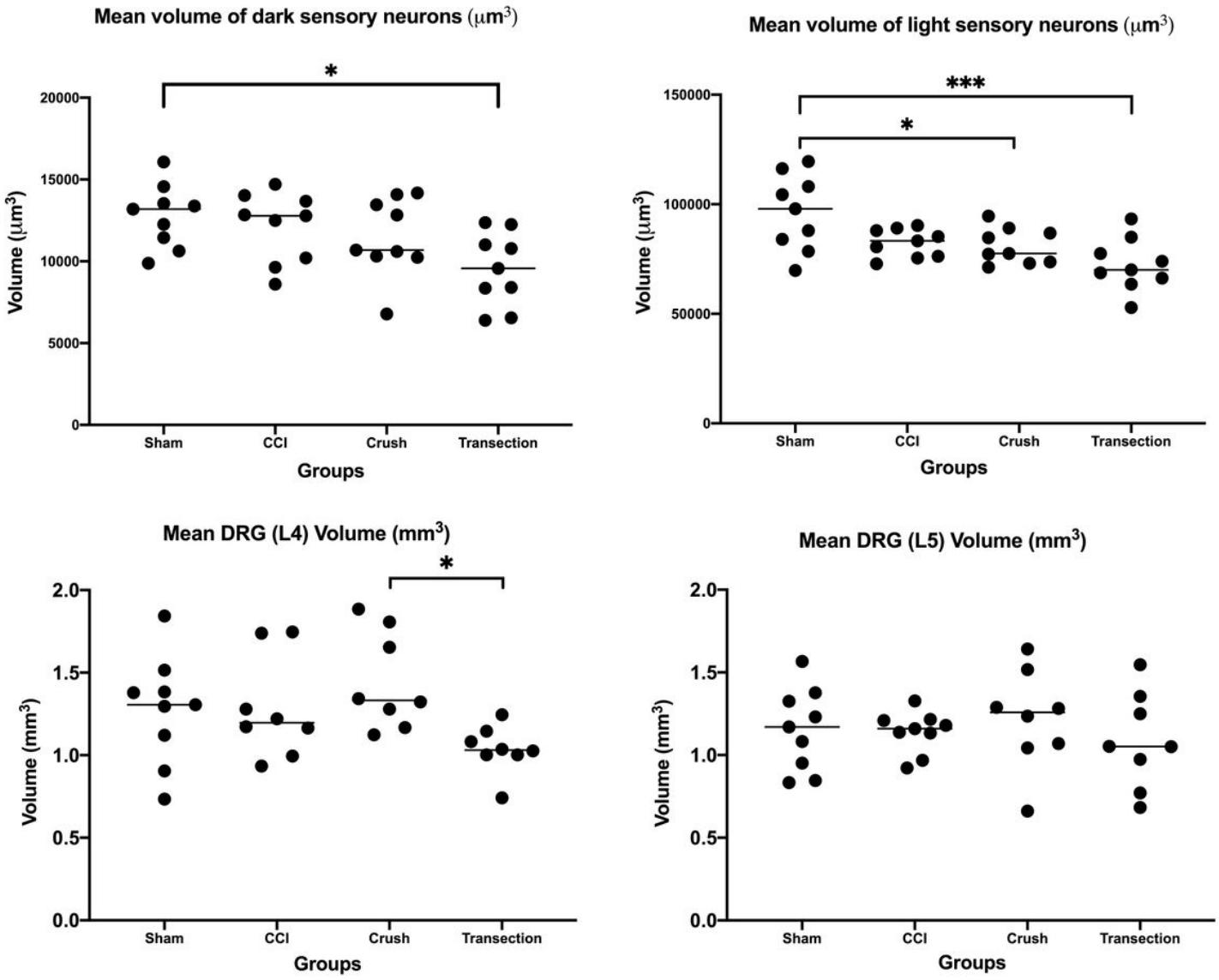

Figure 4

Graphs showing the mean volumes of dark and light sensory neurons and the total mean volumes of the ganglion tissues

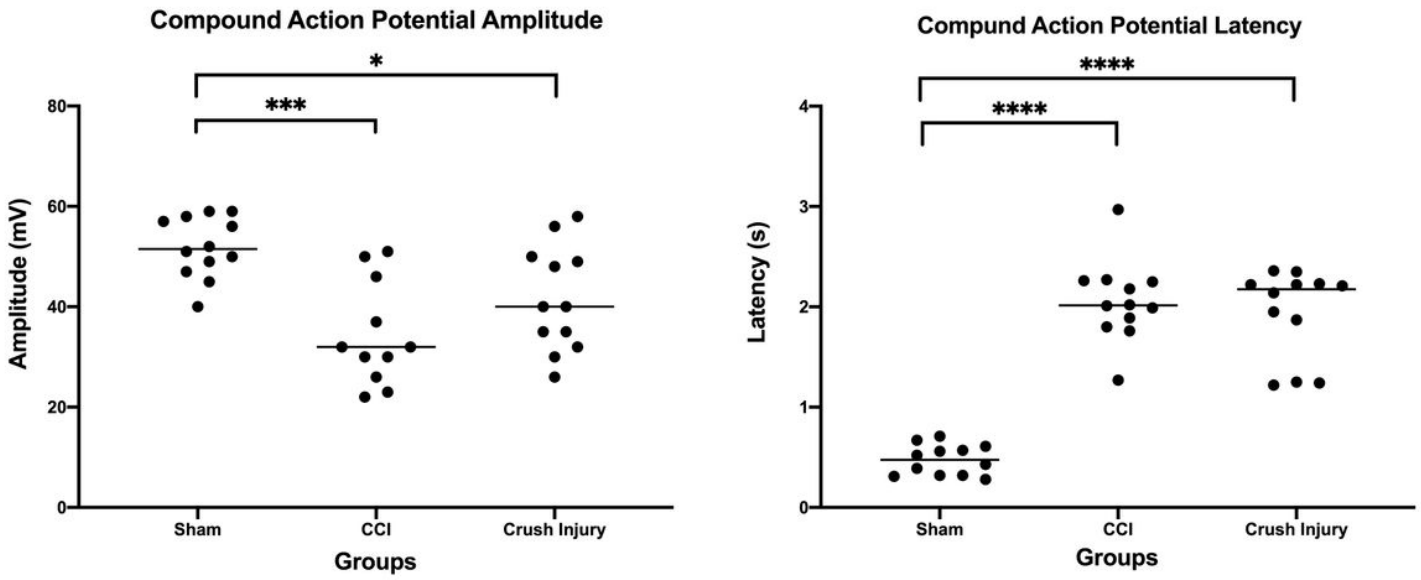

Figure 5

Graphs showing the groups' combined action potential latency (s) and amplitude (mV)

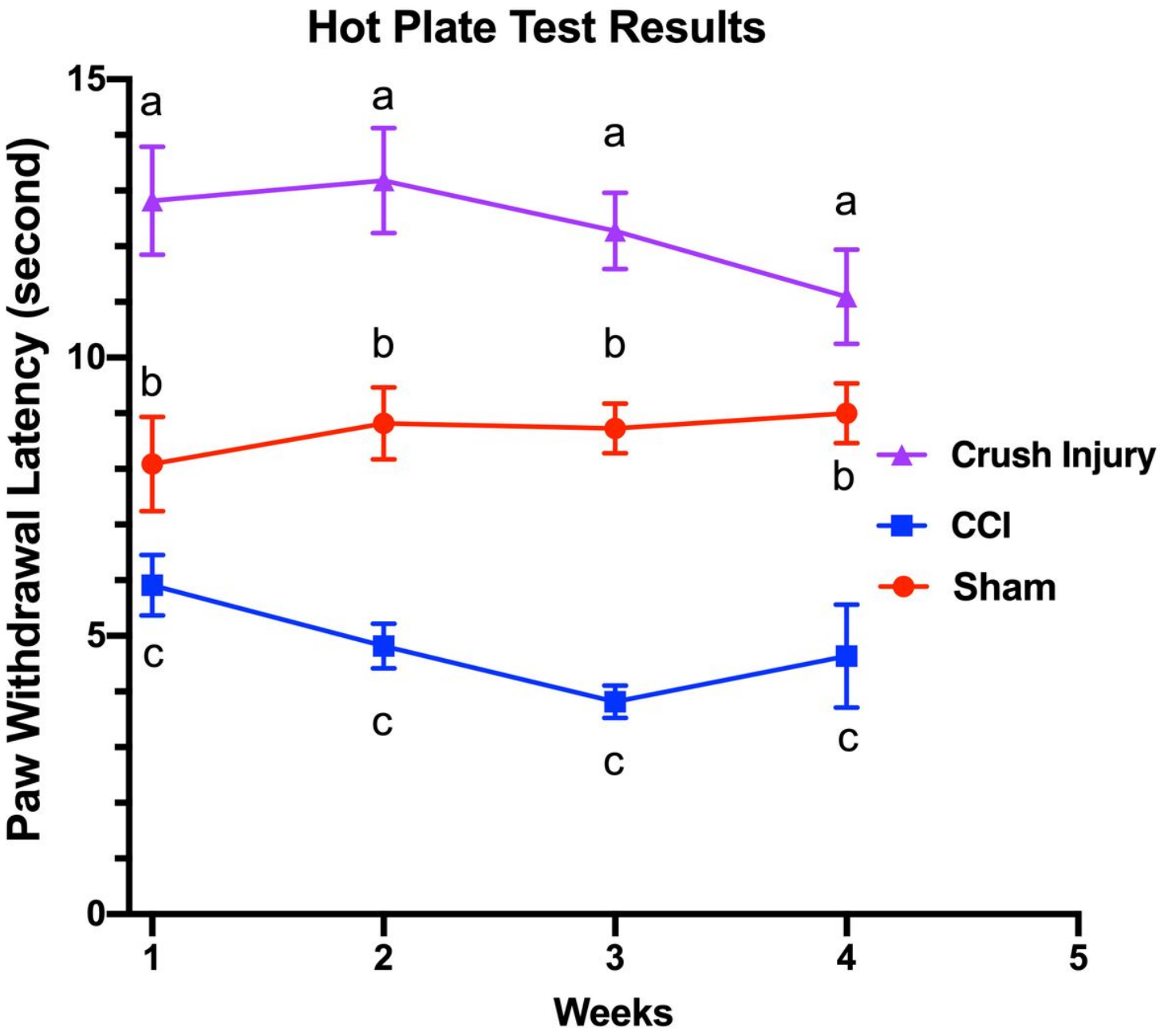

Figure 6

Hot plate test results. Groups that differed statistically within the same week are indicated with different letters (a, b, c)

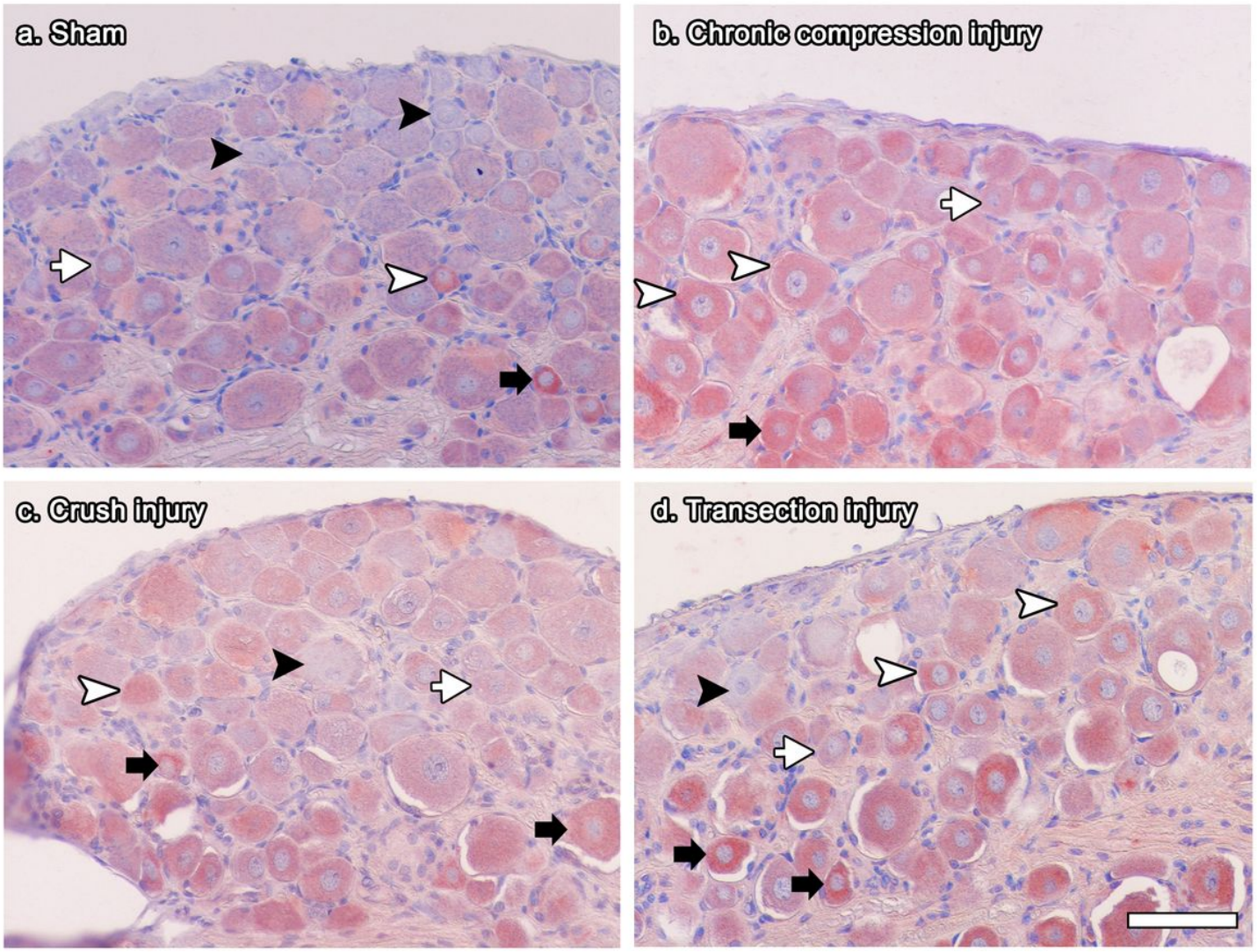

Figure 7

Image showing sections stained with active caspase-3 antibody from the study groups. Positivity was mostly determined in the cytoplasm of large- and small-diameter sensory neurons. Immunopositivity was scored as no staining (0 score) (dark arrowheads), weak staining (+1) (white arrows), moderate staining (+2) (white arrowheads), and intense staining (+3 score) (dark arrows). The sections were counterstained using Mayer's hematoxylin (bar:100 µm)

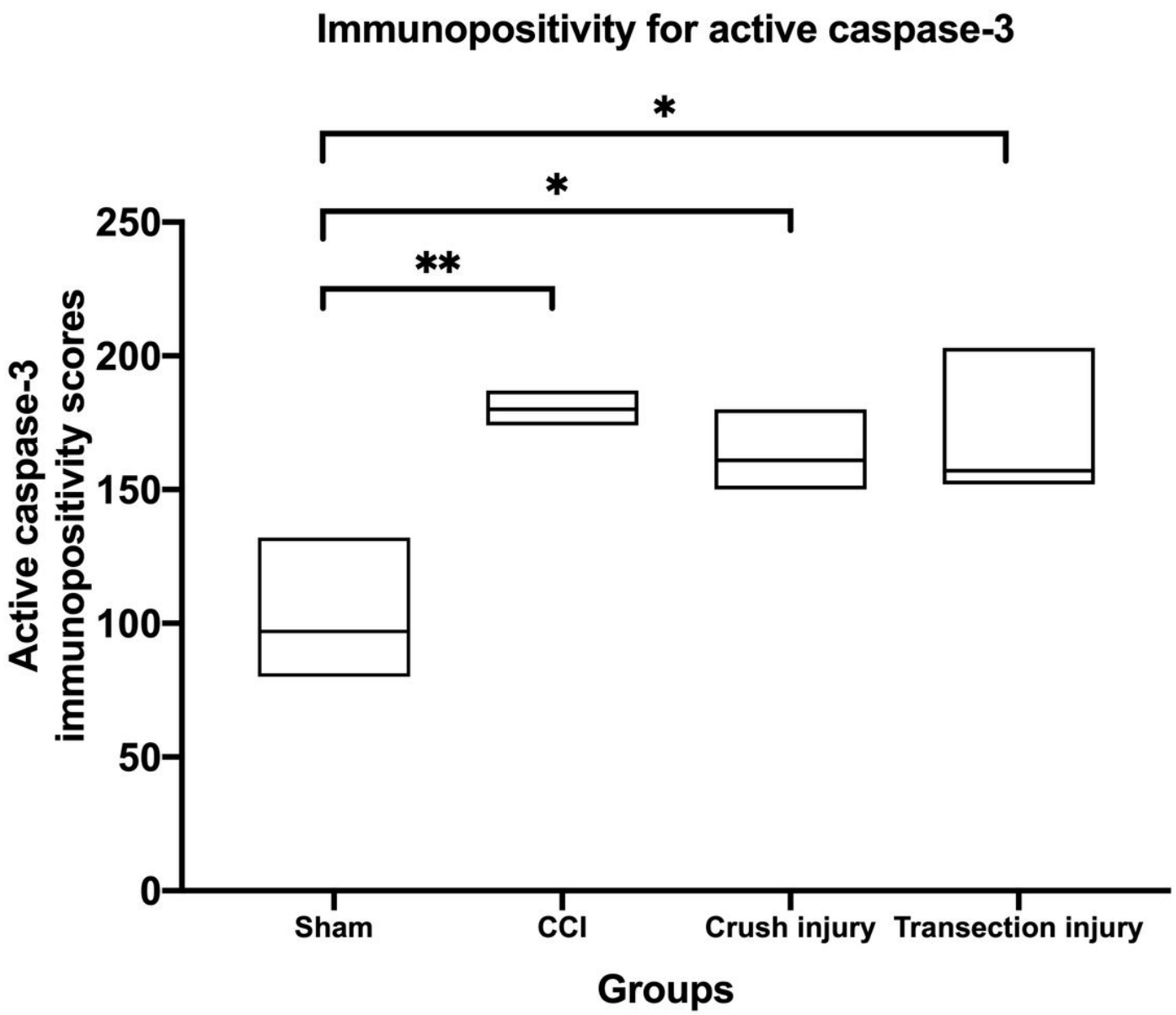

Figure 8

The groups' immunohistochemical scores for active caspase-3 antibody *p<0.05 **p<0.01

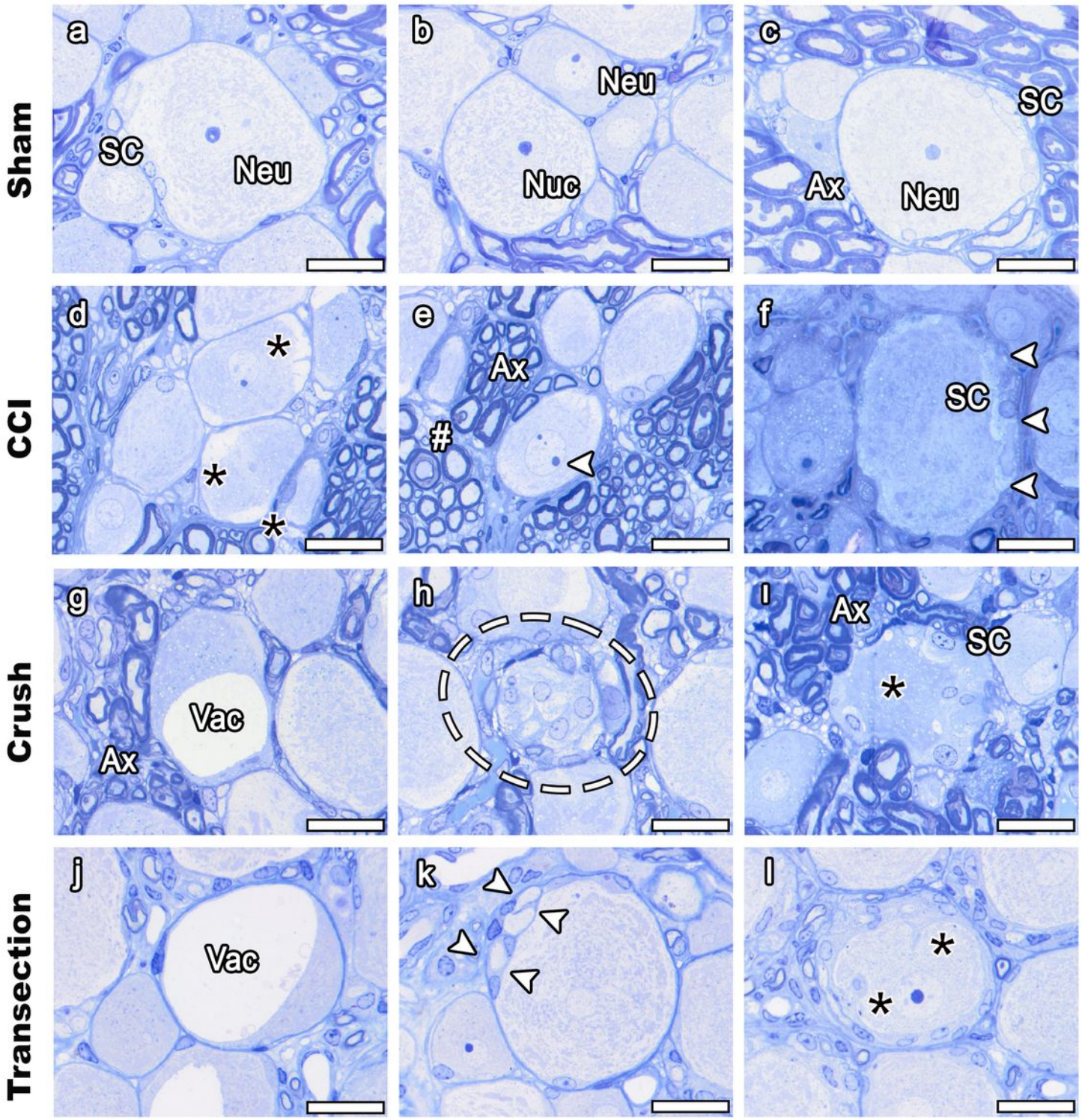

Figure 9

(**a**) Sensory neurons (**Neu**) from the sham group and the satellite cells (**SC**) surrounding them. (**b**) The cell membranes, nuclei (**Nuc**) and nucleolus structures of sensory neurons were all intact. (**c**) Axonal structures (**Ax**) exhibited a normal morphology. (**d**) The dorsal root ganglion from the chronic compression injury group exhibits regional deteriorations in the cytoplasmic integrity of sensory neurons (*). (**e**) Regional structural ballooning (**#**) in the myelin sheath structure of axons is also noteworthy. The

nucleus of the indicated sensory neuron is in an eccentric position (**arrowhead**). (**f**) Hypertrophy was evident in the satellite cells (**arrowhead**). (**g**) The crush group exhibited widened areas of vacuolization in the cytoplasm of the sensory neurons occupying most of the cytoplasmic area (**Vac**). Deteriorations can also be seen in the axonal structural integrity (**Ax**). (**h**) A sensory neuron thought to have been newly phagocyted can be seen in the marked area (**dashed line**). (**ı**) The sensory neuron marked (*) in the figure is thought to have been phagocytized by the surrounding phagocytic cells. Volume increase (**SC**) and phagocytic cell-like structural changes in satellite cells are also noteworthy. Structural deteriorations of axons (**Ax**) are evident. (**j**) Large areas of vacuolization (**Vac**) covering most of the cytoplasm can be seen in some neurons. (**k**) Areas of vacuolization were also found in the cytoplasm of some satellite cells (**arrowhead**). (**l**) Autophagosomes (*****) originating from satellite cells displaying phagocytic cell behavior produce extensions toward the cytoplasm of a sensory neuron(toluidine blue staining) Bar:30 µm

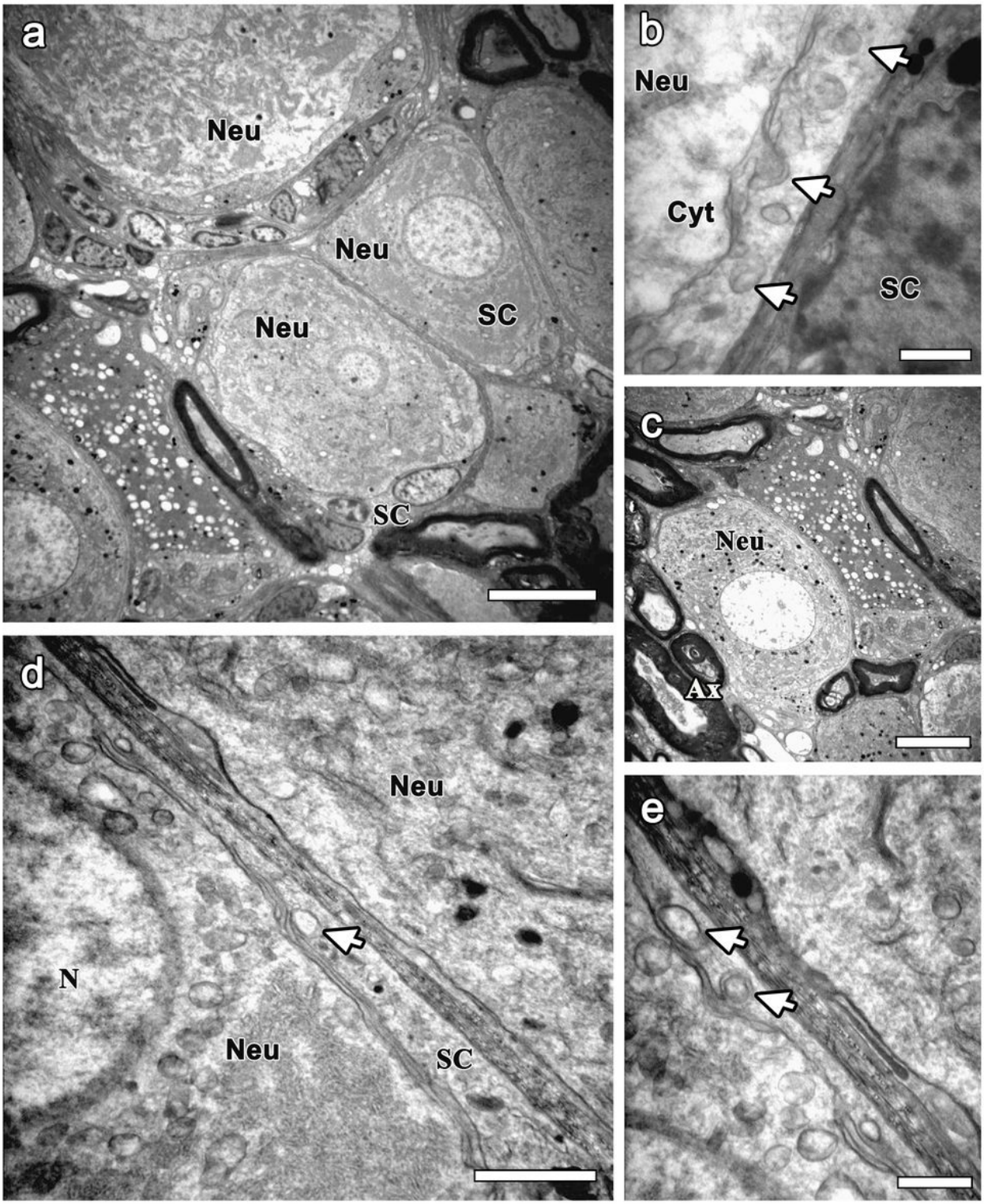

Figure 10

(**a**) Images showing sensory neurons (**Neu**) and satellite cells (**SC**) from the sham group (bar:10 μm). (**b**) The interdigitation area between a sensory neuron (**Neu**) and the surrounding satellite cell can be seen under high magnification. The satellite cell produces indentations toward the sensory neuron cytoplasm and facilitates the transportation of substances between the cytoplasms of the two cells (**arrow**) (bar:1 μm). (**c**) The sensory neurons (**Neu**) and axons (**Ax**) were intact (bar:10 μm). (**d, e**) Cellular changes can

be seen between the neuron and satellite cell cytoplasm. The phagosome structure with a lipid bilayer membrane can be observed in the satellite cell cytoplasm (**arrow**). Bars: **a**, 10 μm; **b**, 1 μm; **c**, 10 μm; **d**, 1 μm; **e**, 2 μm

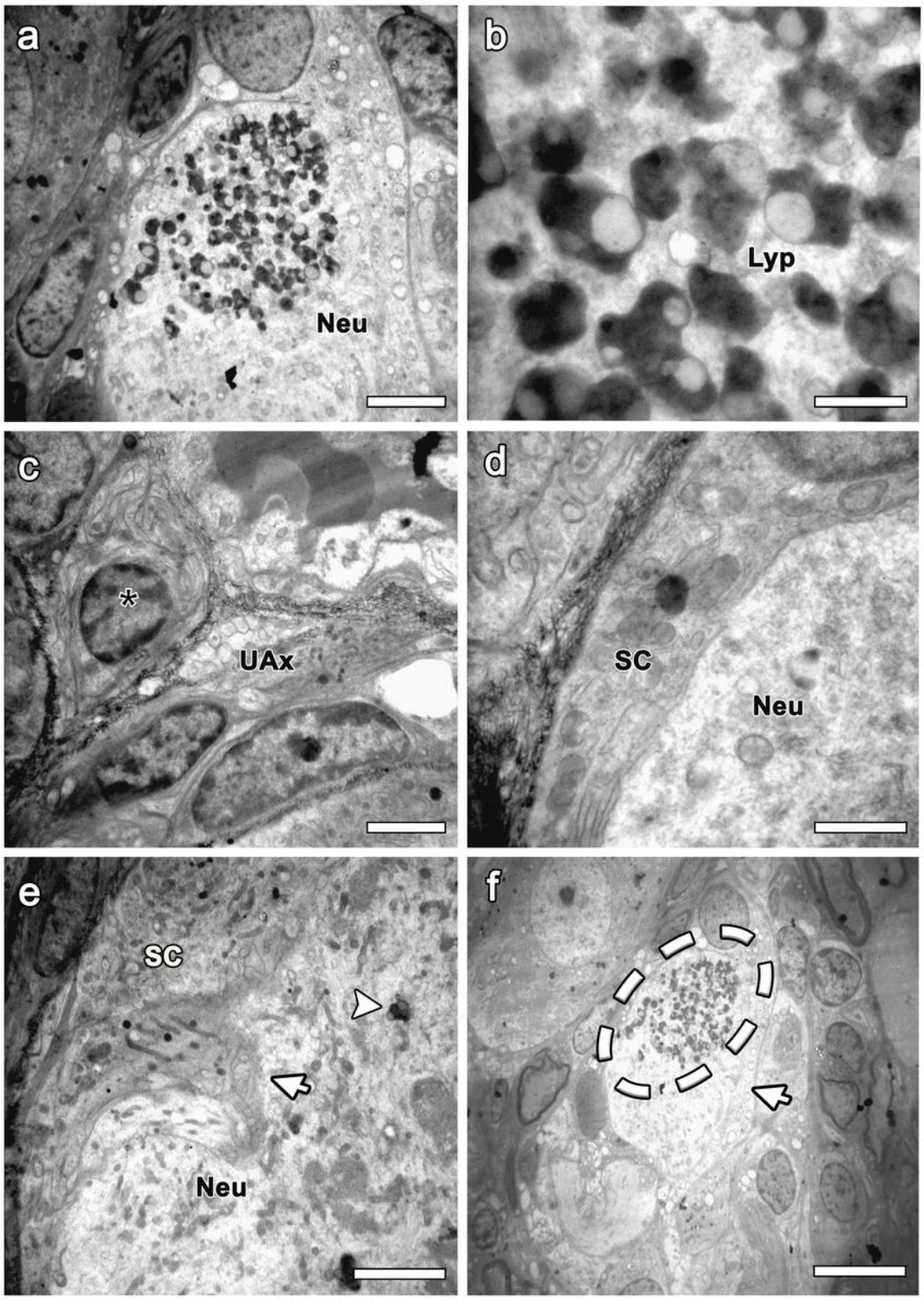

Figure 11

(**a, b**) Representative photographs from the chronic compression injury group. Lipofuscin (**Lyp**) granules accumulated eccentrically in the cytoplasm of the neuron (**Neu**). (**c**) A plasma-like cell (**asterisk**) located in the connective tissue is seen. (**d**) Hypertrophy was observed in the cytoplasm of the satellite cell. (**e**) The cytoplasmic extension (**arrow**) of the satellite cell towards the cytoplasm of the neuron draws attention. Lipofuscin granules (**arrowhead**) containing lipid droplets were shown with an arrowhead. (**f**) A large number of lipofuscin granules were evident in the cytoplasm, concentrated in the periphery of the cytoplasm (**dashed lines**). Bars: **a**, 4 µm; **b**, 1 µm; **c**, 2 µm; **d**, 1 µm; **e**, 4 µm; **f**, 10 µm

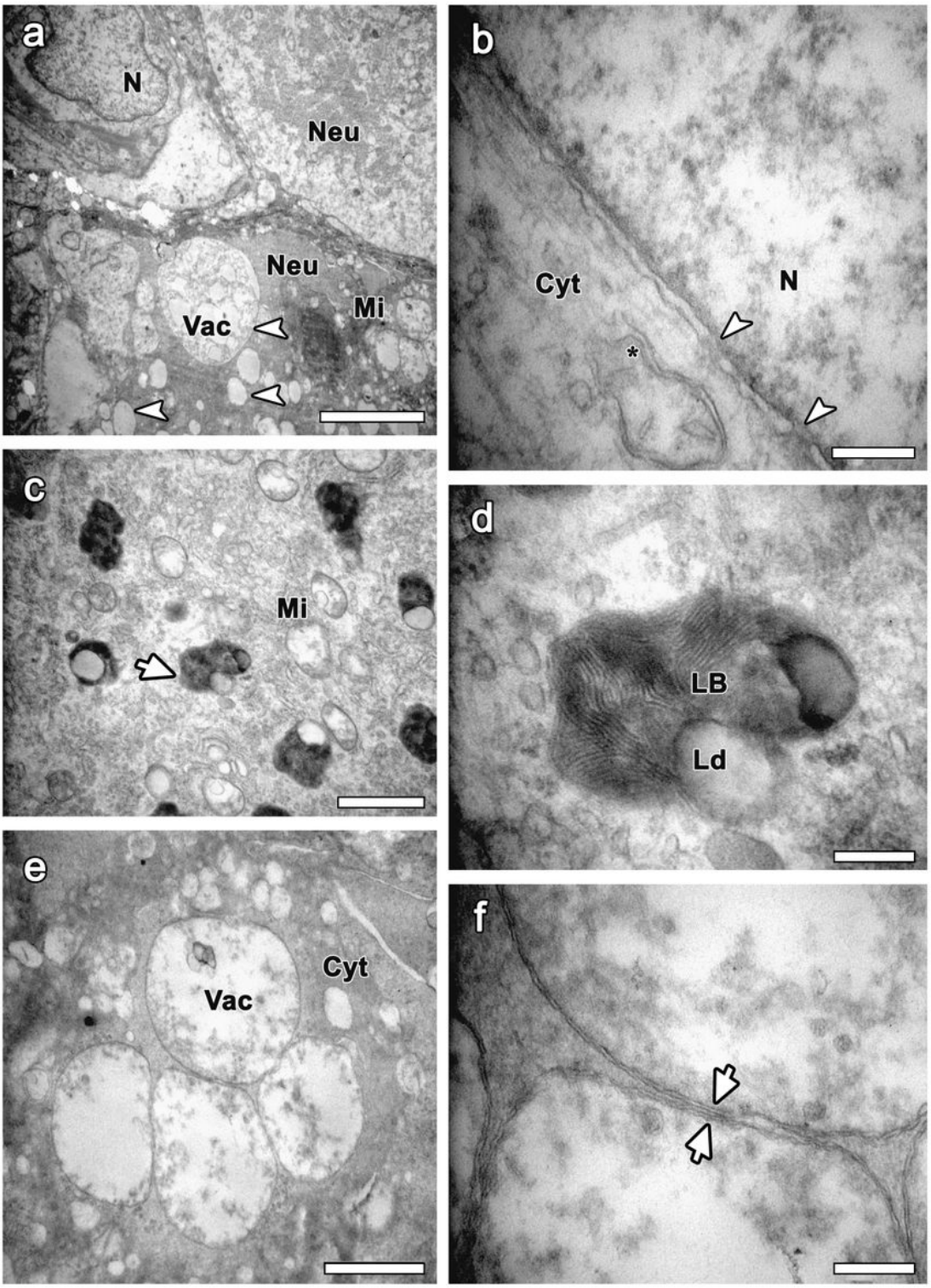

Figure 12

(**a**) Images from the crush injury group. Structural deteriorations in the cytoplasm of the sensory neurons, vacuolization areas (**Vac**), and swollen mitochondria (**Mi**) can be seen (**arrowhead**). **(b)** Nuclear pores located in the nucleus of the sensory neuron (**N**) are indicated by an arrow and regional deteriorations in the inner cristae of mitochondria are particularly remarkable (*****). (**c**) Lipofuscin granules (**arrow**) are clearly visible in addition to an increase in organelle density and disruptions in mitochondrial structures (**Mi**). **(d)** The presence of lamellar bodies (**LB**) and lipid droplet (**Ld**) in the electron-dense region of the granules are noteworthy. (**e, f**) The lipid bilayer structure of autophagic vacuoles (**Vac**) in the cytoplasm of some sensory neurons is indicated by arrows. Bars: **a**, 4 μm; **b**, 200 nm; **c**, 1 μm; **d**, 200 nm; **e**, 1 μm; **f**, 200 nm

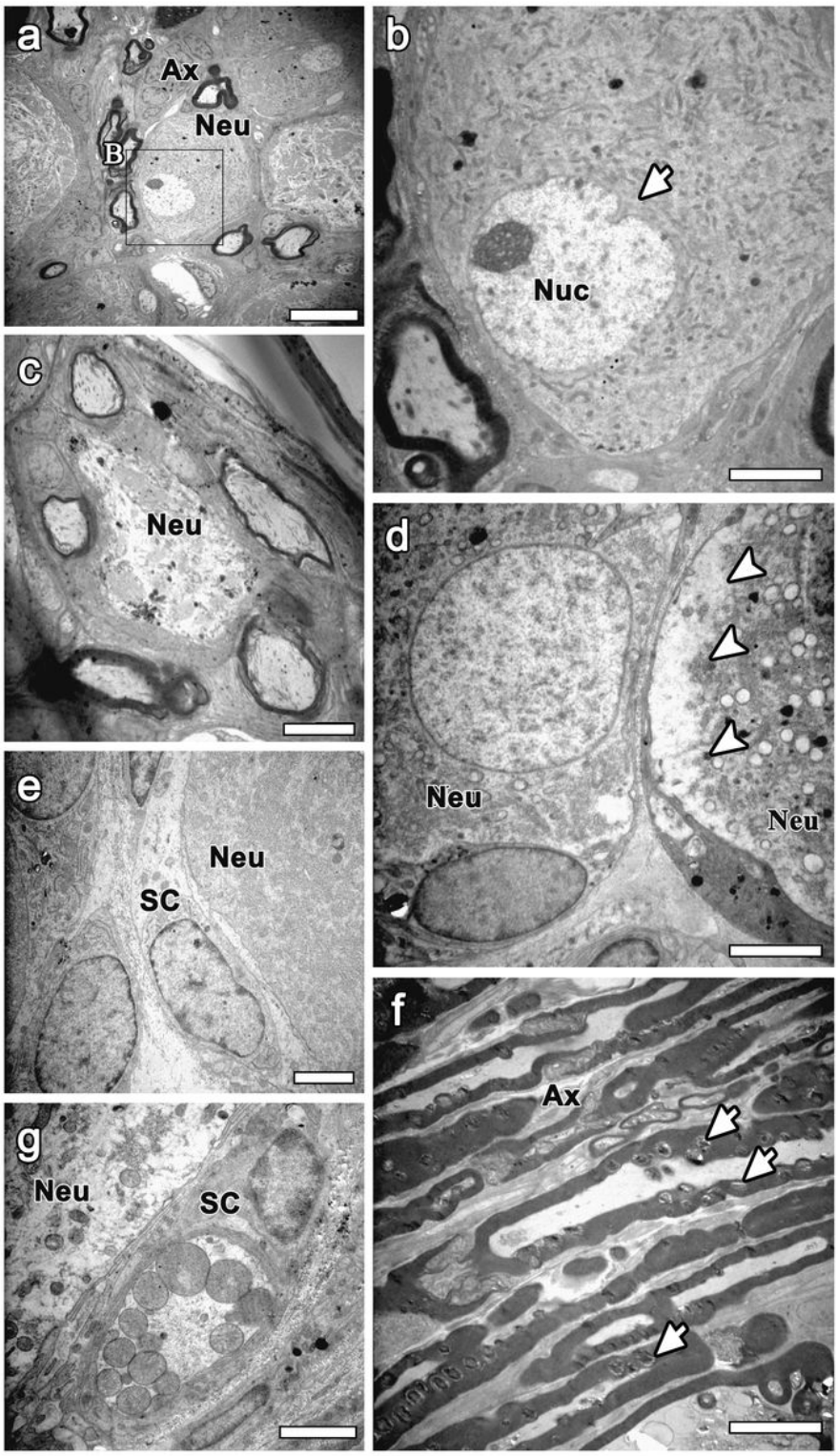

Figure 13

Images of the sensory neurons (**Neu**) from the transection injury group. (**a**) Variation can be seen in the organelle distribution and nuclear structures of the sensory neurons. (**b**) The arrow shows an indented nucleus. (**c**) This photo shows a sensory neuron (**Neu**) surrounded by satellite cells / phagocytic cells. Swollen axons can be seen in close proximity to the sensory neuron. (**d**) Deterioration is visible in the cytoplasm of the sensory neuron (**Neu**). **(e)** Hypertrophy in the cytoplasm of the satellite cell is

particularly noteworthy. (**f**) Regional thawing can be seen in the myelin sheath of the axons. (**g**) Mitochondria surrounded by a vacuole are visible in the cytoplasm of a satellite cell. Bars: **a**, 10 μm; **b**, 4 μm; **c**, 10 μm; **d**, 4 μm; **e**, 2 μm; **f**, 10 μm; g, 2 μm

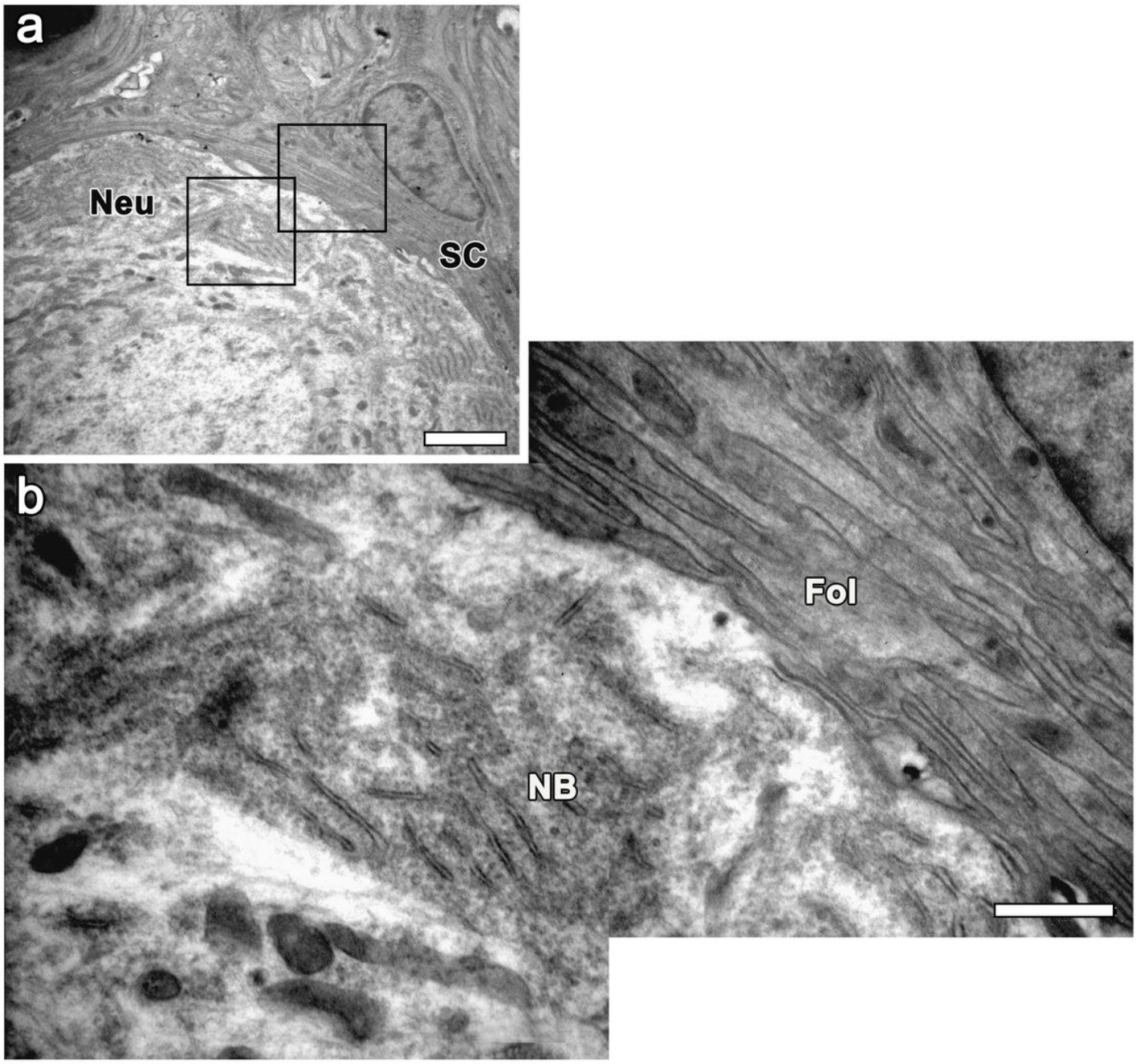

Figure 14

Images from the transection injury group. (**a**) Chromatolysis resulting from transection injury is clearly visible in the sensory neurons (**Neu**). The Nissl bodies are in an eccentric location (**NB**). (**b**) Folding patterns (**Fol**) is noteworthy in the satellite cell membrane. Bars: **a**, 4 μm; **b**, 1 μm

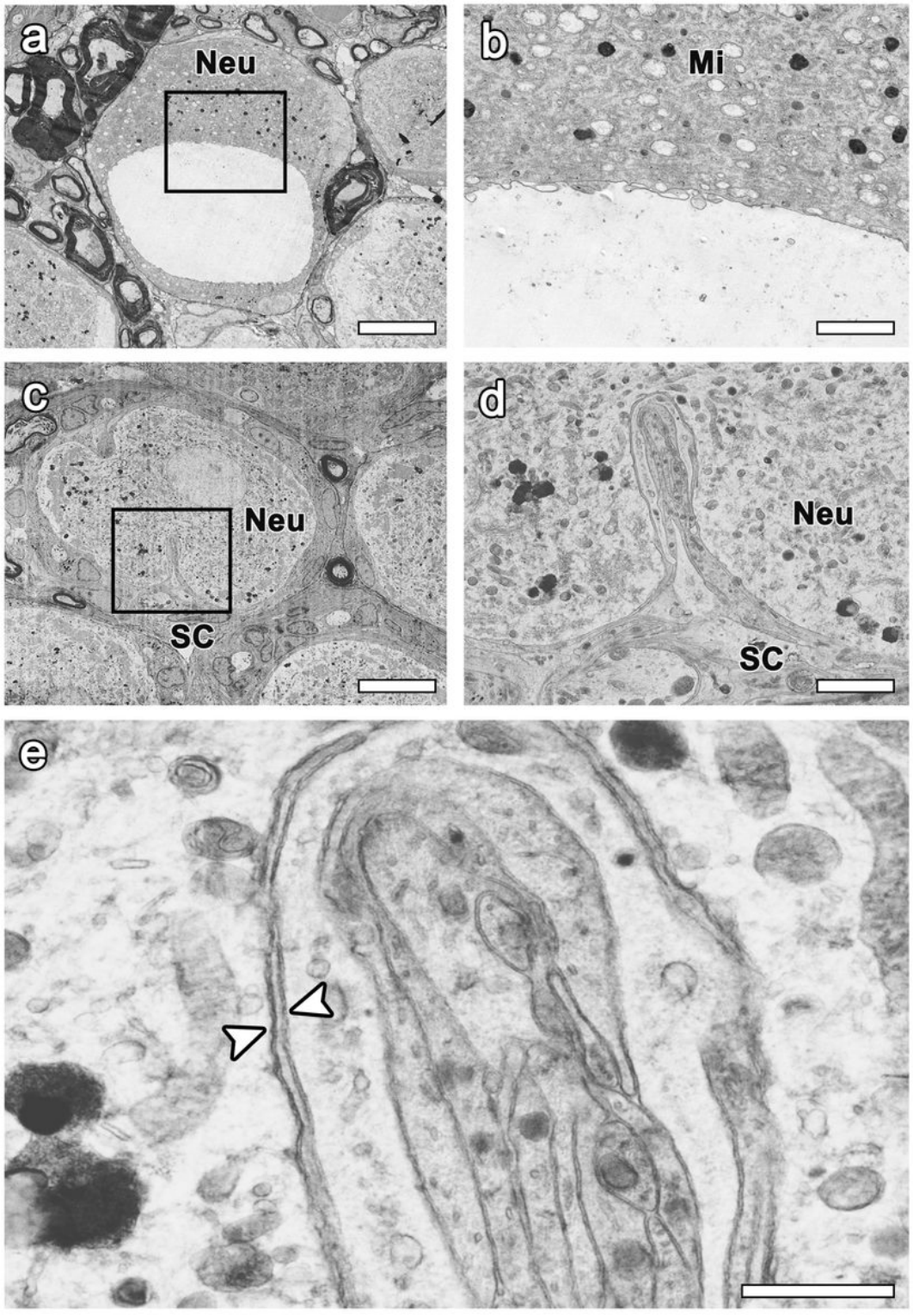

Figure 15

Images from the transection injury group. (**a**) Widened vacuolization areas are clearly visible in the cytoplasm of the sensory neurons. (**b**) The area in the **box** (**Fig. a**) can be seen under high magnification. The vacuole is surrounded by a thin membrane. The inner cristae of the mitochondria (Mi) is disrupted. (**c**) Invagination of the glia cell (**SC**) into the neuron cytoplasm is shown in the box. (**d**) The lipid bilayer of

a coiled phagophore can be seen at high magnification. (**e**) The lipid bilayer of the phagophore is indicated by arrows. Bars: **a**, 10 μm; **b**, 2 μm; **c**, 10 μm; **d**, 1 μm; **e**, 500 nm